An Efficient Multilayer Approach to Model DNA-Based Nano-Biosensors

Jesús Lucia-Tamudo,[†] Juan J. Nogueira,[*,†,‡] and Sergio Díaz-Tendero[*,†,‡,¶]

†*Department of Chemistry, Universidad Autónoma de Madrid, 28049, Madrid, Spain*

‡*Institute for Advanced Research in Chemistry (IAdChem), Universidad Autónoma de Madrid, 28049 Madrid, Spain*

¶*Condensed Matter Physics Center (IFIMAC), Universidad Autónoma de Madrid, 28049 Madrid, Spain*

E-mail: juan.nogueira@uam.es; sergio.diaztendero@uam.es

Abstract

In this work we present a full computational protocol to successfully obtain the one-electron reduction potential of nano-biosensors based on a self-assembled monolayer of DNA nucleobases linked to a gold substrate. The model is able to account for conformational sampling and environmental effects at a quantum mechanical (QM) level efficiently, by combining classical molecular dynamics (MM) and multilayer QM/MM/continuum calculations within the framework of Marcus theory. The theoretical model shows that a guanine-based biosensor is more prone to be oxidized than the isolated nucleobase in water due to the electrostatic interactions between the assembled guanine molecules. In addition, the redox properties of the biosensor can be tuned by modifying the nature of the linker that anchor the nucleobases to the metal support.

Biosensors are nowadays one of the most powerful tools for detecting the presence of specific analytes and determining their concentrations in a given sample.[1,2] In fact, biosensors

are widely used in many fields such as health service,[2–10] control assurance,[1,11–14] environmental science,[2,15] biology,[16,17] and many others. These analytical devices are able to convert a biochemical signal, e.g., modification of the levels of a biospecies of interest, into a measurable signal. Generally, their operation mode is the following (see Figure 1a): Firstly, the analyte is trapped by the bioreceptor due to chemical or physical interactions. Then, the raw signal is sent to the transducer and transformed into an appropriate signal to be read by the signal processing device. The nature of this measurable signal can be electrochemical,[18–20] magnetic,[21–23] optical,[24–27] piezoelectric,[16] or thermal,[2] among others. Furthermore, the intensity of the signal must be proportional to the amount of analyte in the sample to obtain adequate detection.

Due to the wide range of constituents in terms of their nature and the selected analytical technique for the detection, there is a huge amount of possible combinations to design a biosensor.[2] Focusing on the bioreceptor, the key point for its selection resides on the fact that it cannot lose its properties once it is integrated into the sensor. Otherwise, the analyte could not interact with the bioreceptor as it usually does, when the latter is in its free form. In addition, the bioreceptor must be chosen selectively in order to respond only to one specific analyte or one class of analytes. Bioreceptors tipically employed are enzymes, immunosensors, bioreceptors based on polymers, DNA or nucleobases, tissues or even organelles.[2–4,15–17]

Electrochemical techniques are the most popular choice to measure the transformed signal for the detection task due to their low cost, portability, simplicity of construction, straightforward use, high sensibility and selectivity.[19,20,28–33] Within this group of devices, there is a large variety of methods that can be employed for signal procesing: voltammetry, amperometry, potentiometry, conductimetry, spectroscopy of electrochemical impedance, and so on. Recently, electrochemical DNA-based biosensors have become a convenient choice when trying to detect specific sequencies of nucleic acids, heavy metal ions, organic molecules, as well as using them as nanowires.[34–41] This type of biosensors consists of an ensemble of

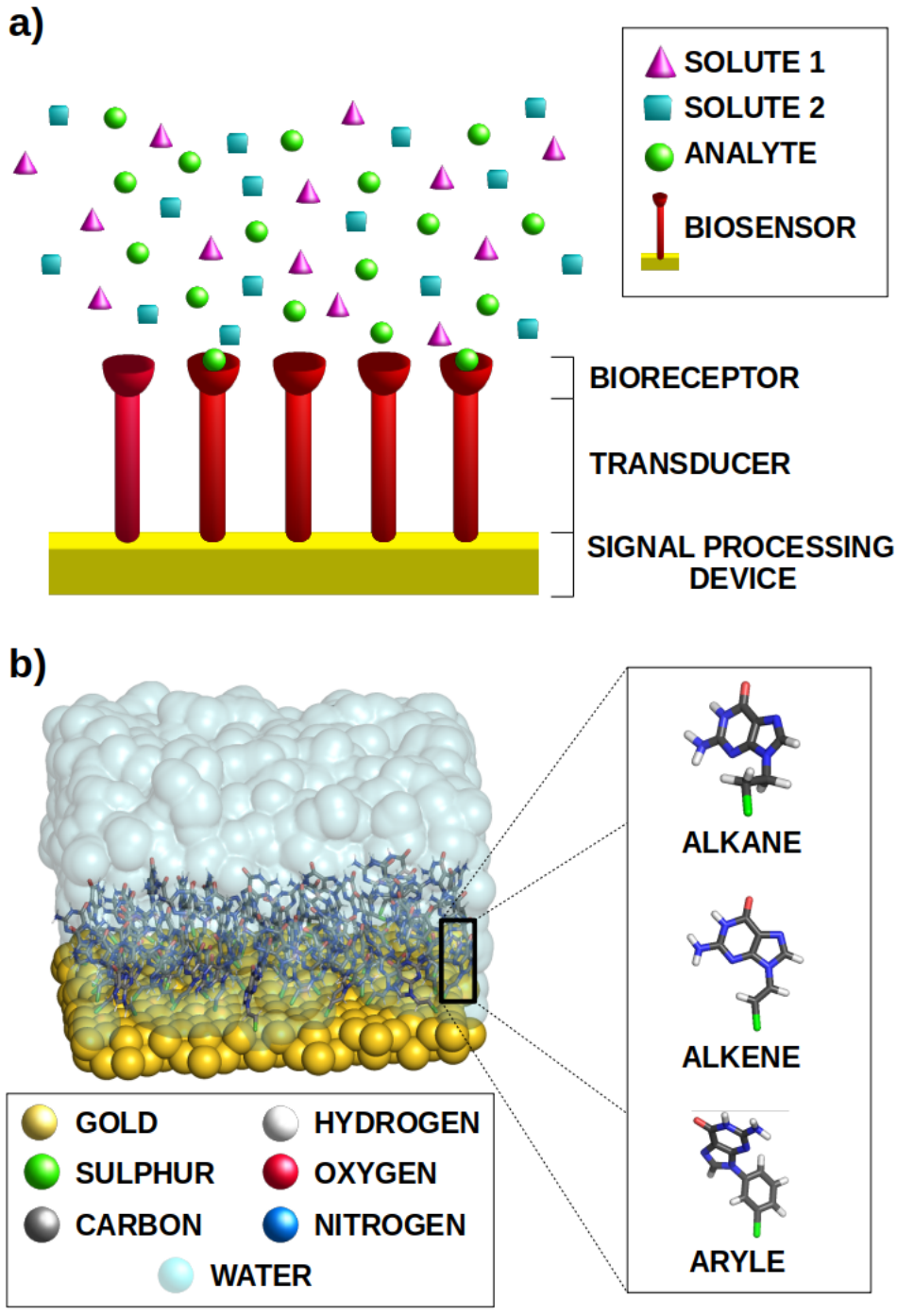

Figure 1: Schematic representation of a) the general structure of a standard biosensor, b) the models employed in this study: an ensemble of guanines anchored to a gold surface by different organic linkers.

single-stranded DNA (ss-DNA) or double-stranded DNA (ds-DNA) molecules adsorbed on a metal surface, constituting a self-assembled monolayer (SAM).[42–45] Several issues must be addressed when designing and emplying these devices. First, the nucleobase is the main moiety responsible for the electron transfer along the DNA strand, and thus, intense research has been aimed to obtain accurate redox properties of nucleobases to understand and characterize the charge-transfer processes that take place on the transmission of the signal along the DNA strand.[46–58] In this context, guanine is the most susceptible nucleobase to be oxidized. Second, the most common metals employed as substrates of SAMs are Au, Ag, Cu, Pt, Hg, Ga, and As. However, not only the nature of the metal but also its crystallographic structural organization plays an important role.[59] In the case of gold surfaces, the most popular and stable crystal orientation are the Au(100) and Au(111) ones. Finally, the interaction between the biosensor and the metal is an important issue. For example, most of the studied SAMs are constituted by a gold substrate covalently bonded to thiolated or selenated organic molecules, since the Au-S(Se) bond is very strong and stabilizes the assembly.[60–62]

Along this study, the one-electron reduction potential of a SAM biosensors formed by guanine molecules anchored to a Au(100) surface by three different linkers, namely, thioalkane, thioaryl, and thioalkene species (see Figure 1b), is investigated by means of computational methods. We will use the term "one-electron reduction potential" as the potential of the oxidation process but considered in the direction of a reduction reaction. Specifically, the variation of the reduction potential of guanine is analyzed when going from the free nucleobase in solution to the SAM assembly. It was found that guanine is more prone to be oxidized when it is part of the SAM and, thus, the redox properties are enhanced for biosensing purposes. Moreover, it was determined that the selection of the linker can module the one-electron reduction potential of the biosensor. From a computational point of view, a protocol to obtain accurate one-electron reduction potentials for SAMs at affordable computational cost was developed and applied.

The system under study (see Figure 1b) is relatively large from the computational point of view (more than 6000 atoms) since the model considers the metal substrate, a SAM formed by the guanine and linker molecules, and water molecules as solvent. This implies that the potential energy surface of the system presents different local minima that can be populated at room temperature and that have to be considered when computing the redox properties. Thus, the first step of the theoretical protocol was to run classical molecular dynamics (MD) simulations to explore the potential energy surface. Then, the one-electron reduction potential was computed for several snapshots selected from the dynamics by hybrid quantum mechanics/molecular mechanics (QM/MM) and QM/MM/continuum computations, where the QM region was treated at density functional theory (DFT) level. The smallest part of the system that should be described quantum mechanically is one of the nucleobases and its linker. We will refer to this smallest QM region as reference ligand (RL). However, the environment surrounding this moiety can significantly affect the value of the reduction potential and, thus, it could also be necessary to consider additional parts of the system to be included in the QM region. It is possible to distinguish three different components in the SAM: the ensemble of nucleobases with their linkers, the gold surface and the solvent. The effect of including each of this components in the QM region on the one-electron reduction potential is investigated here (see Figure 2). A more detailed description of the methods and the computational details are given in the Supporting Information.

We start by analyzing the effect of the gold atoms on the reduction potential of the system. Since the linker that connects the nucleobase and the metallic substrate is small, the guanine/gold nonbonded interactions can be strong and influence the electronic properties of the nucleobase. Therefore, the evaluation of the the ligand-surface interactions is important. Figure 2a shows the effect of introducing an increasing number of gold atoms in the QM region for five geometries randomly selected from the dynamics. The first two gold atoms considered are the closest ones to the sulphur atom of the RL unit located on the upper layer of the metal substrate. The following two gold atoms to be treated quantum mechanically

are the nearest ones to the sulphur atom, which are located on the lower layer of the gold surface. The last four gold atoms were chosen to be the adjacent atoms to the two first selected gold atoms on the upper layer of the surface. The results revealed that there is a significant decrease of the reduction potential when an increasing number of gold atoms are included in the QM region. The potential reaches convergence when four gold atoms are described at QM level. If the attention is focused on the location of gold atoms of the QM region along the surface, the lower shell of the surface still modify the redox properties of the ligand. This might be a consequence of the coupling between the electronic clouds of the upper and lower layers of the metal and its effect on the sulphur-gold bond, which in turn modifies the reduction potential of guanine. In fact, it seems that the inclusion of the gold atoms of the lower layer is even more relevant than the upper one for some of the geometries (e.g., frames 3 and 4). In terms of convergence and computational cost, including four gold atoms in the QM region seems to be the best option.

From a parallel perspective, the way that the solvent is described can influence the computed value of the one-electron reduction potential of the guanine nucleobase embedded in the SAM. The solvent can be described by explicit and implicit models in QM/MM and QM/continuum calculations, respectively.[63] To analyze the behaviour of the reduction potential with explicit solvation, the same five geometries used above were also analyzed. Specifically, an increasing number water molecules up to 60 were included in the QM region together with the RL, while the remaining water molecules were described by the TIP3P force field (see Figure 2b). In general terms, the QM/MM potential experiences an increase in its value when the first 10 water molecules are considered in the QM region. Then, from 10 to 20 QM water molecules the potential decreases and, finally, becomes constant for larger QM region sizes. Therefore, the description of 20 water molecules in the QM layer is enough to reach a converged value of the reduction potential. In addition, a description of the solvent through the continuum COSMO solvation model was also considered.[64,65] Despite their limitations related to the lack of atomic resolution, QM/continuum schemes imply three

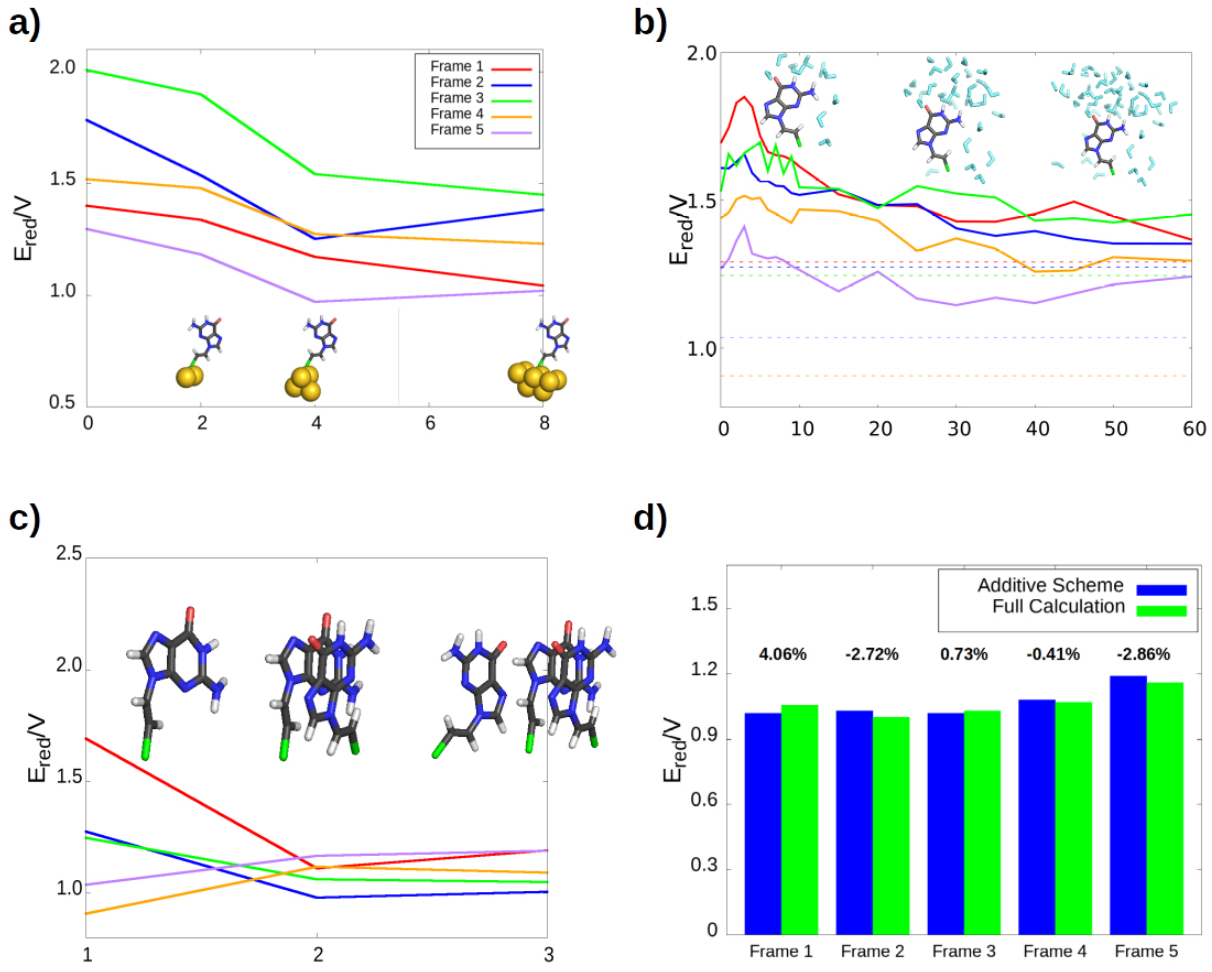

Figure 2: Variation of the one-electron reduction potential with an increasing number of a) gold atoms, b) water molecules, and c) organic molecules (nucleobase + linker) in the QM region. Each colour line represents a single snapshot obtained from the MD trajectory. Panel b) also shows the values of the reduction potential as dashed lines when the COSMO implicit model is used as solvent. d) Validation of the additive scheme compared to a full QM/MM calculation (see text).

clear advantages over a QM/MM description: (i) The QM region becomes smaller since all the solvent molecules are described by the continuum model; since a lower computational cost is required other components can be included in the QM region. (ii) The COSMO approach is a polarizable solvent model in which both the solvent and the solute polarize each other in a self-consistent manner, leading to a better description of the solute/solvent interactions. (iii) A continuum model as COSMO represents an average configuration of the solvent, not an explicit one, and, therefore, a smaller number of snapshots is needed to obtain converged results for ensemble of geometries. The dashed lines displayed in Figure 2b shows the values of the computed reduction potential for each of the five geometries analyzed above using COSMO to describe the solvent. As can be seen, when implicit solvation is employed the reduction potential is smaller than that for explicit solvation, especially for the frames 4 and 5. This can be a consequence of the better description of the interactions and the averaging nature of the model as mentioned above.

The third component of the device is the organic monolayer (SAM) formed by the guanine and linker molecules (the ligands). Due to the aromatic character of the ligands, with large electronic π-systems, it will not be surprising that the interactions between them can modify the value of the one-electron reduction potential of the system. Thus, the addition of neighbour molecules to the RL moiety in the QM layer can be of paramount importance for the determination of the potential. The same procedure as those explained above for metal atoms and water molecules was also applied for ligands (see Figure 2c). It is important to highlight that the positive charge of the cationic species during the QM/MM calculations within the Marcus theory (see the Supporting Information) was restrained to be in the guanine of the RL. This means that charge delocalization among different ligands has not been taken into account, since it is out of the scope of this work. However, delocalization effects could be relevant and need to be addressed in future research. Figure 2c shows that the addition of the closest ligand to the RL has a big impact on the value of the reduction potential. This is clearly due to a response to the interactions between π-systems of adjacent

molecules. The addition of a third ligand into the QM region does not affect the value of the potential and, thus, the inclusion of only one ligand in the QM layer, in addition of the reference one, is enough to account for these interactions.

The inspection of Figures 2a-c provides the ideal size of the QM region: two ligands, four gold atoms and 20 water molecules. However, these results also give rise to a conflict. All these elements in the QM region would lead to highly expensive calculations that are not worthy to afford. To alleviate the computational cost, the solvent will be described by COSMO since, as discussed above, represents a good choice to reduce the number of calculations and to improve the solute/solvent bulk interactions. Despite the application of the continuum solvent model, performing QM/MM/COSMO calculations where the QM region is formed by two ligands and four gold atoms (and the MM region by the remaining ligands and gold atoms) is still computationally unfeasible, especially considering that hundreds of geometries have to be taken into account to obtain converged results. Therefore, an alternative protocol with lower computational cost must be set. In this context, it was tested whether the effect of the individual components of the biosensor to the reduction potential can be considered additive or not. If this is the case, the one-electron reduction potential for the largest QM region (two ligands and four gold atoms) can be written as the sum of the potential for a model where only one ligand composes the QM region plus gold and ligand effects, which are computed by using reduced QM regions (one ligand and four gold atoms for a set of calculations and two ligands for the other):

$$\Delta E_{red,2L-4Au} = \Delta E_{red,1L} + (\Delta E_{red,1L-4Au} - \Delta E_{red,1L}) + (\Delta E_{red,2L} - \Delta E_{red,1L}) \qquad (1)$$

The calculation of the left-hand term of Eq. (1) is computationally demanding. Thus, the reliability of this additive protocol will be evaluated by taking as reference QM/MM calculations where the QM region is formed by only two gold atoms and two ligands. However, once the additive scheme is shown to be correct (see below), the right-hand side of Eq. (1)

(including four gold atoms in the QM region) will be applied to compute in a more accurate way the potential of the biosensor. Therefore, for the purpose of the evaluation of the additive scheme, Eq. (1) converts into Eq. (2):

$$\Delta E_{red,2L-2Au} = \Delta E_{red,1L} + (\Delta E_{red,1L-2Au} - \Delta E_{red,1L}) + (\Delta E_{red,2L} - \Delta E_{red,1L}) \qquad (2)$$

The subscripts iL and iAu refer to the number of ligands and gold atoms considered in the QM region, respectively. Figure 2d compares the additive scheme (right-hand terms of Eq. (2)) with the so-called full QM calculation (left-hand term of Eq. (2)). The potentials obtained from both sets of calculations were pretty similar, giving evidence that the additive protocol is valid. Differences between potential values for each considered geometry were almost negligible. In all the cases, the relative error of the additive potentials with respect to the full calculation was less than 5%. Therefore, the additive scheme was applied to reduce the QM region size and the computational cost in the following calculations where a large ensemble of snapshots is considered.

In the next step, the following procedure was performed to compute the one-electron oxidation potential of the biosensor taking into account conformational sampling. First of all, classical MD simulations were run for both the neutral and the localized monocationic versions of the SAM, in which only one nucleobase molecule is positively charged. After reaching the equilibrium, 200 geometries were randomly fetched from the trajectory. For each geometry, the three reduction potentials of the right-hand side of Eq. (1), using different QM region sizes, are computed by applying the Marcus theory, as previously done.[58] In all the cases, the positive charge was restrained to be located on the guanine molecule of the RL. As said above, solvent effects were included with the COSMO model, and the remaining components of each situation were described by MM point charges, giving rise to a multilayer QM/MM/COSMO scheme. Finally, applying Eq.(1) and averaging over the 200 snapshots, the one-electron reduction potential of the system was then determined. These calculations

were performed for three different biosensors which differ in the linker that anchors the guanine to the gold surface: ethane, ethene and aryle. In order to choose the linkers, a set of static calculations were performed for simplify models formed by guanine, different linkers and COSMO solvent (see Supporting Information). The one-electron reduction potential of these models was calculated using the direct static approach established in a previous work.[58] The range of the potentials obtained for the different linkers was small: $0.99 - 1.28$ V. Thus, there is not a big influence of the linker bonded to the free guanine nucleobase in solution. The question here is whether this dependence enlarges or not when the ligand is anchored into a gold surface forming a SAM, where an organic environment and a gold surface also interacting with the RL. This was investigated for three linkers of different nature: alkane, alkene and aryle.

Figure 3 shows the one-electron reduction potentials obtained for each of the three organic species in both situations: free molecule in an aqueous solvent (red bars) and the molecule as part of a solvated SAM (purple bars). The second situation was obtained using the additive scheme, as described above. As said before, it can be seen that when the three species are free in solvent their one-electron reduction potentials are similar: the difference between the most oxidant and the most reducer species is less than 0.1 V (see also Supporting Information). Consequently, the linker does not affect the redox properties of the guanine residue significantly when the nucleobase is in solvent. However, this situation changes when each of the organic ligands are embedded into a SAM. The most susceptible system to oxidation, which is the SAM whose linker is an aryle group, shows a one-electron reduction potential almost 0.5 V lower than the SAM with the alkene linker. Therefore, the presence of an environment –refereed to the gold surface and the organic part of the SAM– plays an important role in the redox properties of a single molecule. Even when the additive scheme is not applied and only one ligand is described at a quantum-mechanical level of theory, the differences in their redox properties are clearly evident (blue bars). In fact, the contributions added from the introduction of gold atoms and other ligands in the QM region

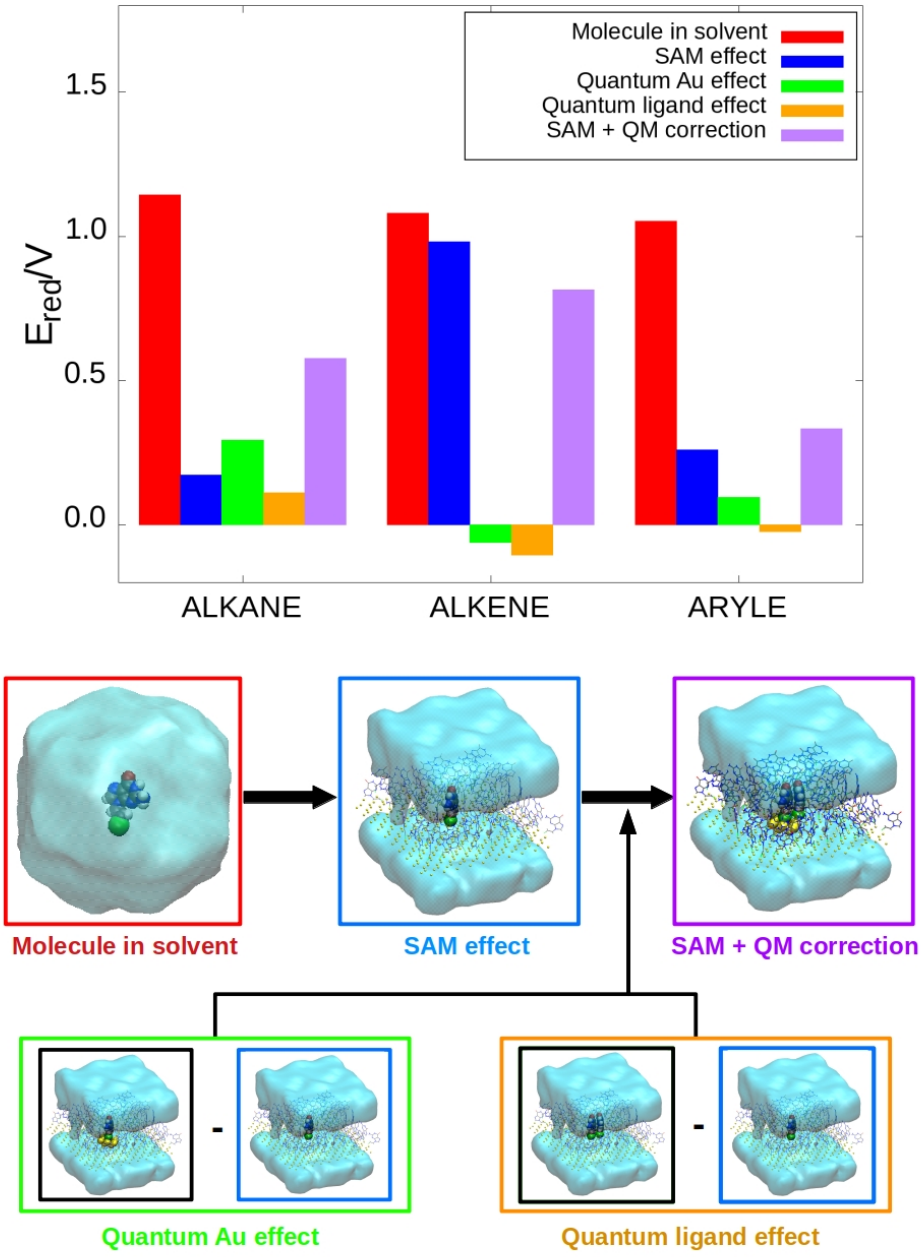

Figure 3: One-electron reduction potential of a guanine residue when it is free in water solution (red bar), it is placed on a SAM which is described by a force field (blue bar), iii) the additive scheme is applied (purple bar). The quantum contributions to the additive scheme of the gold (green bar) and ligand (orange bar) moieties are shown. The schematic representation below the plot shows graphically the process to apply the additive scheme (Eq. (1)). Colour code for the atoms and solvent: sulphur in green, carbon in gray, nitrogen in blue, oxygen in red, hydrogen in white, gold in yellow and the solvent in aquamarine.

generally modify in small quantities the values of the redox potentials. This means that the effect of the environment on the reduction potential of the biosensor is already described in a reasonable way by a classical force field, and the introduction of part of the environment in the QM region is needed only to quantitatively refine the value of the potential.

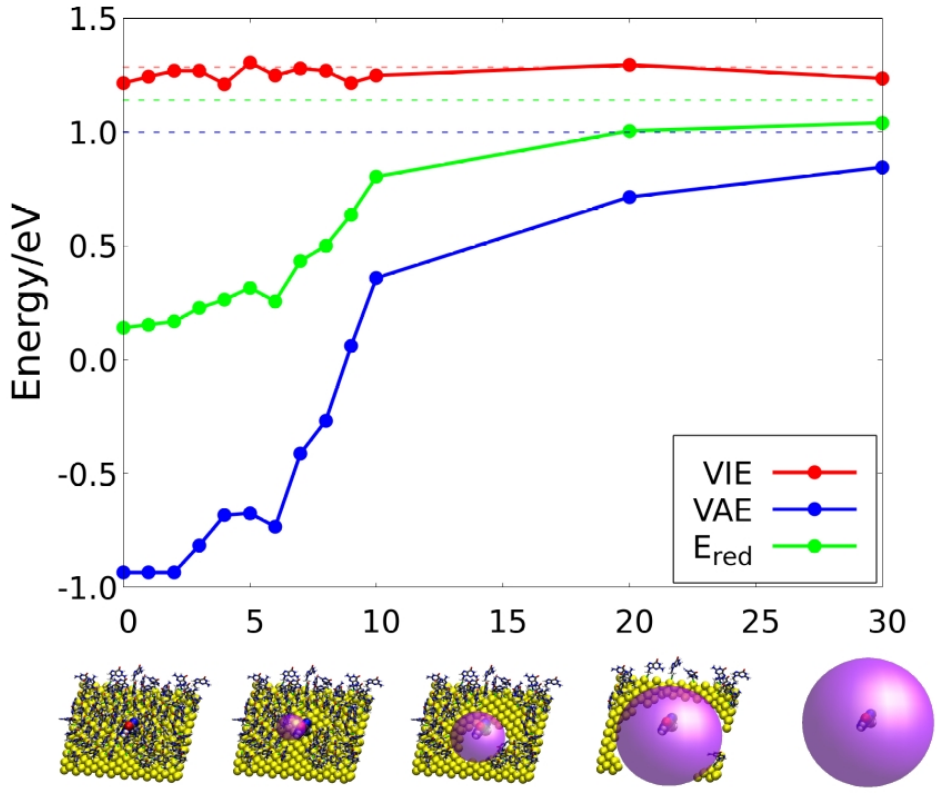

Figure 4: Schematic representation of the calculations performed to study the decrease of the one-electron reduction potential as the environment is taken into account closer to the reference ligand. The solvent is always describied using COSMO. The vacuum bubble generated between the classical charges and the QM region is represented by the purple sphere. Colour code: gold in yellow, nitrogen in blue, oxygen in red, carbon in gray, hydrogen in white, sulphur in green.

The role of the environment can be analyzed in more detail in Figure 3 by comparing the variation of the potential when going from aqueous solvent (red bar) to the SAM environment (purple bar). The one-electron reduction potential drastically drops in the SAM. Specifically, the potentials of the SAM with the alkane, alkene and aryle linkers decrease 0.97 V, 0.10

V and 0.79 V, respectively, with respect to the molecule in solvent. This means that the reducer character of the guanine-linker complex increases due to the electrostatic interactions with the other components of the SAM. In addition, as mentioned above, this behaviour is qualitatively reproduced when the environment is described classically (blue bar). This means that the drop in the potential is caused mostly by the interactions with the organic ligands and not with the gold atoms, since the electrostatic interactions with the latter are predicted to be zero by the force field. In order to corroborate the importance of the electrostatic interactions with the organic region of the SAM, a set of calculations were carried out in which the MM charges of the environment were added from a farther to a nearer radius with respect to the RL (see Figure 4 from right to left). We show this analysis for the case of the alkane linker because its one-electron reduction potential in the SAM is the most influenced by the SAM with respect to the molecule in solvent. The results revealed that the vertical ionization energy (VIE) remains constant with the addition of nearer point charges. However, the vertical electron affinity (VEA) decreases considerably as nearer ligands are placed around the RL and, therefore, the reduction potentials also decreases. This trend is also observed in the aryle case and in a lower extent for the alkene linker. Therefore, the electrostatic interactions between the organic fragments of the SAM (nucleobases and linkers) induce an important decrease of the reduction potential of the biosensor.

In summary, the redox properties for guanine are extremely affected by the molecular environment. When the nucleobase is free in aqueous medium its potential barely changes by the organic linker. This suggest that the predominant interactions with water, which are similar no matter which liker is bonded to the guanine nucleobase, regulates the redox properties of the system. However, the value of the potential is highly altered when the guanine is part of a SAM with equivalent molecules anchored to a gold surface. Firstly, the introduction of other neighbour ligands decreases the reduction potential, forming a system in which oxidation is more probable to occur. As a result, the redox properties of guanine are

enhanced when it is integrated into a SAM, leading to a promising model for a DNA-based biosensor. Secondly, the nature of the linker that assembles the guanine molecules to the gold surface also affects significantly the one-electron reduction potential. Consequently, it is possible to tune the redox properties of the nucleobases by choosing an appropriate linker, which can be used to improve the selectivity of the device. Finally, this study presents an efficient computational strategy that can be employed to obtain reduction potentials for very large systems at quantum mechanical level of accuracy by applying an additive scheme in a computationally affordable manner. Such a theoretical model can help to rationally design new nano-biosensors with tuned redox properties.

Acknowledgement

We acknowledge the generous allocation of computer time at the Centro de Computación Científica at the Universidad Autónoma de Madrid (CCC-UAM). This work was partially supported by the MICINN - Spanish Ministry of Science and Innovation – Projects PID2019-110091GB-I00 and PID2020-117806GA-I00 funded by MCIN/AEI/10.13039/501100011033, and the 'María de Maeztu' (CEX2018-000805-M) Program for Centers of Excellence in R&D. J.J.N. acknowledge the Comunidad de Madrid for funding through the Attraction of Talent Program (Grant ref 2018-T1/BMD-10261). J.L.T. acknowledges the FPU-2019 grant from the Spanish Ministry of University.

References

(1) Kissinger, P. T. Biosensors—a perspective. *Biosens. Bioelectron.* **2005**, *20*, 2512–2516.

(2) Mehrotra, P. Biosensors and their applications – A review. *J. Oral Biol. Craniofac. Res.* **2016**, *6*, 153–159.

(3) Devasenathipathy, R.; Mani, V.; Chen, S. M.; Huang, S. T.; Huang, T. T.; Lin, C. M.;

Hwa, K. Y.; Chen, T. Y.; Chen, B. J. Glucose biosensor based on glucose oxidase immobilized at gold nanoparticles decorated graphene-carbon nanotubes. *Enzyme Microb. Technol.* **2015**, *78*, 40–45.

(4) Jönsson, G.; Gorton, L. An amperometric glucose sensor made by modification of a graphite electrode surface with immobilized glucose oxidase and adsorbed mediator. *Biosensors* **1985**, *1*, 355–368.

(5) Lee, M.; Zine, N.; Baraket, A.; Zabala, M.; Campabadal, F.; Caruso, R.; Trivella, M. G.; Jaffrezic-Renault, N.; Errachid, A. A novel biosensor based on hafnium oxide: Application for early stage detection of human interleukin-10. *Sens. Actuators B Chem.* **2012**, *175*, 201–207.

(6) Lu, S.; Wang, Y. Fluorescence Resonance Energy Transfer Biosensors for Cancer Detection and Evaluation of Drug Efficacy. *Clin. Cancer Res.* **2010**, *16*, 3822 – 3824.

(7) Wang, J. Electrochemical biosensors: Towards point-of-care cancer diagnostics. *Biosens. Bioelectron.* **2006**, *21*, 1887–1892.

(8) Huang, H.; Bai, W.; Dong, C.; Guo, R.; Liu, Z. An ultrasensitive electrochemical DNA biosensor based on graphene/Au nanorod/polythionine for human papillomavirus DNA detection. *Biosens. Bioelectron.* **2015**, *68*, 442–446.

(9) Frew, J. E.; Hill, H. A. O.; Thomas, J. D. R.; Akhtar, M.; Lowe, C. R.; Higgins, I. J. Electron-transfer biosensors. *Philos. Trans. R. Soc. Lond., B, Biol. Sci.* **1987**, *316*, 95–106.

(10) Burcu Bahadır, E.; Kemal Sezgintürk, M. Applications of electrochemical immunosensors for early clinical diagnostics. *Talanta* **2015**, *132*, 162–174.

(11) Ghasemi-Varnamkhasti, M.; Rodríguez-Méndez, M. L.; Mohtasebi, S. S.; Apetrei, C.;

Lozano, J.; Ahmadi, H.; Razavi, S. H.; de Saja, J. A. Monitoring the aging of beers using a bioelectronic tongue. *Food Control* **2012**, *25*, 216–224.

(12) Bäcker, M.; Rakowski, D.; Poghossian, A.; Biselli, M.; Wagner, P.; Schöning, M. Chip-based amperometric enzyme sensor system for monitoring of bioprocesses by flow-injection analysis. *J. Biotechnol.* **2013**, *163*, 371–376.

(13) Ercole, C.; Del Gallo, M.; Mosiello, L.; Baccella, S.; Lepidi, A. Escherichia coli detection in vegetable food by a potentiometric biosensor. *Sens. Actuators B Chem.* **2003**, *91*, 163–168.

(14) Luong, J. H.; Bouvrette, P.; Male, K. B. Developments and applications of biosensors in food analysis. *Trends Biotechnol.* **1997**, *15*, 369–377.

(15) Gui, R.; Jin, H.; Guo, H.; Wang, Z. Recent advances and future prospects in molecularly imprinted polymers-based electrochemical biosensors. *Biosens. Bioelectron.* **2018**, *100*, 56–70.

(16) Pohanka, M. QCM immunosensor for the determination of Staphylococcus aureus antigen. *Chem. Pap.* **2019**, *74*, 451 – 458.

(17) Wijesuriya, D.; Rechnitz, G. Biosensors based on plant and animal tissues. *Biosens. Bioelectron.* **1993**, *8*, 155–160.

(18) Vogiazi, V.; de la Cruz, A.; Mishra, S.; Shanov, V.; Heineman, W. R.; Dionysiou, D. D. A Comprehensive Review: Development of Electrochemical Biosensors for Detection of Cyanotoxins in Freshwater. *ACS Sensors* **2019**, *4*, 1151–1173.

(19) Mehrvar, M.; Abdi, M. Recent Developments, Characteristics, and Potential Applications of Electrochemical Biosensors. *Anal Sci.* **2004**, *20*, 1113–1126.

(20) Thévenot, D. R.; Toth, K.; Durst, R. A.; Wilson, G. S. Electrochemical biosensors: recommended definitions and classification. *Biosens. Bioelectron.* **2001**, *16*, 121–131.

(21) Yang, Y.; Lin, L.; Zhang, Y.; Jing, Q.; Hou, T.-C.; Wang, Z. L. Self-Powered Magnetic Sensor Based on a Triboelectric Nanogenerator. *ACS Nano* **2012**, *6*, 10378–10383.

(22) Wang, Z.; Xianyu, Y.; Zhang, Z.; Guo, A.; Li, X.; Dong, Y.; Chen, Y. Background Signal-Free Magnetic Bioassay for Food-Borne Pathogen and Residue of Veterinary Drug via Mn(VII)/Mn(II) Interconversion. *ACS Sensors* **2019**, *4*, 2771–2777.

(23) Scognamiglio, V.; Arduini, F.; Palleschi, G.; Rea, G. Biosensing technology for sustainable food safety. *Trends Anal. Chem.* **2014**, *62*, 1–10.

(24) Vilela, P.; El-Sagheer, A.; Millar, T. M.; Brown, T.; Muskens, O. L.; Kanaras, A. G. Graphene Oxide-Upconversion Nanoparticle Based Optical Sensors for Targeted Detection of mRNA Biomarkers Present in Alzheimer's Disease and Prostate Cancer. *ACS Sensors* **2017**, *2*, 52–56.

(25) Frankaer, C. G.; Rosenberg, M.; Santella, M.; Hussain, K. J.; Laursen, B. W.; Sørensen, T. J. Tuning the pKa of a pH Responsive Fluorophore and the Consequences for Calibration of Optical Sensors Based on a Single Fluorophore but Multiple Receptors. *ACS Sensors* **2019**, *4*, 764–773.

(26) Leatherbarrow, R. J.; Edwards, P. R. Analysis of molecular recognition using optical biosensors. *Curr. Opin. Chem. Biol.* **1999**, *3*, 544–547.

(27) Minunni, M.; Tombelli, S.; Mascini, M.; Bilia, A.; Bergonzi, M. C.; Vincieri, F. An optical DNA-based biosensor for the analysis of bioactive constituents with application in drug and herbal drug screening. *Talanta* **2005**, *65*, 578–585.

(28) Ronkainen, N. J.; Halsall, H. B.; Heineman, W. R. Electrochemical biosensors. *Chem. Soc. Rev.* **2010**, *39*, 1747–1763.

(29) Grieshaber, D.; MacKenzie, R.; Vörös, J.; Reimhult, E. Electrochemical Biosensors - Sensor Principles and Architectures. *Sensors* **2008**, *8*, 1400–1458.

(30) Pohanka, M.; Skladal, P. Electrochemical biosensors - principles and applications. *J. Appl. Biomed.* **2008**, *6*, 57–64.

(31) Macdonald, J. R. Impedance spectroscopy. *Ann. Biomed. Eng.* **2006**, *20*, 289–305.

(32) Chang, B.-Y.; Park, S.-M. Electrochemical Impedance Spectroscopy. *Annu. Rev. Anal. Chem.* **2010**, *3*, 207–229.

(33) Yu, L.; Zhang, Y.; Hu, C.; Wu, H.; Yang, Y.; Huang, C.; Jia, N. Highly sensitive electrochemical impedance spectroscopy immunosensor for the detection of AFB1 in olive oil. *Food Chem.* **2015**, *176*, 22–26.

(34) Drummond, T. G.; Hill, M. G.; Barton, J. K. Electrochemical DNA sensors. *Nat. Biotechnol.* **2003**, *21*, 1192–1199.

(35) Zhai, J.; Cui, H.; Yang, R. DNA based biosensors. *Biotechnol. Adv.* **1997**, *15*, 43–58.

(36) Ozkan, D.; Kara, P.; Kerman, K.; Meric, B.; Erdem, A.; Jelen, F.; Nielsen, P. E.; Ozsoz, M. DNA and PNA sensing on mercury and carbon electrodes by using methylene blue as an electrochemical label. *Bioelectrochemistry* **2002**, *58*, 119–126.

(37) Liu, A.; Wang, K.; Weng, S.; Lei, Y.; Lin, L.; Chen, W.; Lin, X.; Chen, Y. Development of electrochemical DNA biosensors. *Trends Anal. Chem.* **2012**, *37*, 101–111.

(38) Saidur, M.; Aziz, A. A.; Basirun, W. Recent advances in DNA-based electrochemical biosensors for heavy metal ion detection: A review. *Biosens. Bioelectron.* **2017**, *90*, 125–139.

(39) Bu, N.-N.; Tang, C.-X.; He, X.-W.; Yin, X.-B. Tetrahedron-structured DNA and functional oligonucleotide for construction of an electrochemical DNA-based biosensor. *ChemComm* **2011**, *47*, 7689–7691.

(40) Berlin, Y. A.; Burin, A. L.; Ratner, M. A. DNA as a molecular wire. *Superlattices Microstruct.* **2000**, *28*, 241–252.

(41) Wohlgamuth, C. H.; McWilliams, M. A.; Slinker, J. D. DNA as a Molecular Wire: Distance and Sequence Dependence. *Anal. Chem.* **2013**, *85*, 8634–8640.

(42) Prashar, D. Self Assembled Monolayers -A Review. *Int. J. Chemtech Res.* **2012**, *4*.

(43) Chaki, N. K.; Aslam, M.; Sharma, J.; Vijayamohanan, K. Applications of self-assembled monolayers in materials chemistry. *J. Chem. Sci.* **2001**, *113*, 659–670.

(44) Mandler, D.; Turyan, I. Applications of self-assembled monolayers in electroanalytical chemistry. *Electroanalysis* **1996**, *8*, 207–213.

(45) Mirsky, V. M. New electroanalytical applications of self-assembled monolayers. *Trends Anal. Chem.* **2002**, *21*, 439–450.

(46) D'Annibale, V.; Nardi, A. N.; Amadei, A.; D'Abramo, M. Theoretical Characterization of the Reduction Potentials of Nucleic Acids in Solution. *J. Chem. Theory Comput.* **2021**, *17*, 1301–1307.

(47) Psciuk, B. T.; Lord, R. L.; Munk, B. H.; Schlegel, H. B. Theoretical Determination of One-Electron Oxidation Potentials for Nucleic Acid Bases. *J. Chem. Theory Comput.* **2012**, *8*, 5107–5123.

(48) Faraggi, M.; Broitman, F.; Trent, J. B.; Klapper, M. H. One-Electron Oxidation Reactions of Some Purine and Pyrimidine Bases in Aqueous Solutions. Electrochemical and Pulse Radiolysis Studies. *J. Phys. Chem.* **1996**, *100*, 14751–14761.

(49) Jovanovic, S. V.; Simic, M. G. One-electron redox potentials of purines and pyrimidines. *J. Phys. Chem.* **1986**, *90*, 974–978.

(50) Crespo-Hernández, C. E.; Close, D. M.; Gorb, L.; Leszczynski, J. Determination of Redox Potentials for the Watson-Crick Base Pairs, DNA Nucleosides, and Relevant Nucleoside Analogues. *J. Phys. Chem. B* **2007**, *111*, 5386–5395.

(51) Seidel, C. A. M.; Schulz, A.; Sauer, M. H. M. Nucleobase-Specific Quenching of Fluorescent Dyes. 1. Nucleobase One-Electron Redox Potentials and Their Correlation with Static and Dynamic Quenching Efficiencies. *J. Phys. Chem.* **1996**, *100*, 5541–5553.

(52) Steenken, S.; Jovanovic, S. V. How Easily Oxidizable Is DNA? One-Electron Reduction Potentials of Adenosine and Guanosine Radicals in Aqueous Solution. *J. Am. Chem. Soc.* **1997**, *119*, 617–618.

(53) Steenken, S.; Jovanovic, S. V.; Bietti, M.; Bernhard, K. The Trap Depth (in DNA) of 8-Oxo-7,8-dihydro-2'deoxyguanosine as Derived from Electron-Transfer Equilibria in Aqueous Solution. *J. Am. Chem. Soc.* **2000**, *122*, 2373–2374.

(54) Wang, J.; Yang, S.; Zhang, Y. One-electron oxidation and redox potential of nucleobases and deoxyribonucleosides computed by QM/MM simulations. *Chem. Phys. Lett.* **2020**, *739*, 136948.

(55) Zhang, Y.; Xie, P.; Yang, S.; Han, K. Ionization and Electron Attachment for Nucleobases in Water. *J. Phys. Chem. B* **2019**, *123*, 1237–1247.

(56) Paukku, Y.; Hill, G. Theoretical Determination of One-Electron Redox Potentials for DNA Bases, Base Pairs, and Stacks. *J. Phys. Chem. A* **2011**, *115*, 4804–4810.

(57) Thapa, B.; Schlegel, H. B. Calculations of pKa's and Redox Potentials of Nucleobases with Explicit Waters and Polarizable Continuum Solvation. *J. Phys. Chem. A* **2015**, *119*, 5134–5144.

(58) Lucia-Tamudo, J.; Cárdenas, G.; Anguita-Ortiz, N.; Díaz-Tendero, S.; Nogueira, J. J. Computation of Oxidation Potentials of Solvated Nucleobases by Static and Dynamic Multilayer Approaches. *J. Chem. Inf. Model.* **2022**, *62*, 3365–3380.

(59) Arisnabarreta, N.; Ruano, G. D.; Lingenfelder, M.; Patrito, E. M.; Cometto, F. P.

Comparative Study of the Adsorption of Thiols and Selenols on Au(111) and Au(100). *Langmuir* **2017**, *33*, 13733–13739.

(60) Chevrier, D. M.; Yang, R.; Chatt, A.; Zhang, P. Bonding properties of thiolate-protected gold nanoclusters and structural analogs from X-ray absorption spectroscopy. *Nanotechnol. Rev.* **2015**, *4*, 193–206.

(61) Ciriaco, F.; Mavelli, F.; Cassidei, L. Benchmark calculations of density functionals for organothiol adsorption on gold surfaces. *Comput. Theor. Chem* **2013**, *1009*, 60–69.

(62) Leng, Y. S.; Dyer, P. J.; Krstić, P. S.; Harrison, R. J.; Cummings, P. T. Calibration of chemical bonding between benzenedithiolate and gold: the effects of geometry and size of gold clusters. *Mol. Phys.* **2007**, *105*, 293–300.

(63) Nogueira, J. J.; González, L. Computational Photophysics in the Presence of an Environment. *Annu. Rev. Phys. Chem.* **2018**, *69*, 473–497.

(64) Klamt, A.; Schüürmann, G. COSMO: a new approach to dielectric screening in solvents with explicit expressions for the screening energy and its gradient. *J. Chem. Soc., Perkin Trans. 2* **1993**, 799–805.

(65) York, D. M.; Karplus, M. A Smooth Solvation Potential Based on the Conductor-Like Screening Model. *J. Phys. Chem. A* **1999**, *103*, 11060–11079.